Neural precursor cell-secreted TGF-β2 redirects inflammatory monocyte-derived cells in CNS autoimmunity

Donatella De Feo, Arianna Merlini, Elena Brambilla, Linda Ottoboni, Cecilia Laterza, Ramesh Menon, Sundararajan Srinivasan, Cinthia Farina, Jose Manuel Garcia Manteiga, Erica Butti, Marco Bacigaluppi, Giancarlo Comi, Melanie Greter and Gianvito Martino

SUPPLEMENTAL INFORMATION

SUPPLEMENTAL FIGURES AND SUPPLEMENTAL FIGURE LEGENDS

Supplemental Figure 1

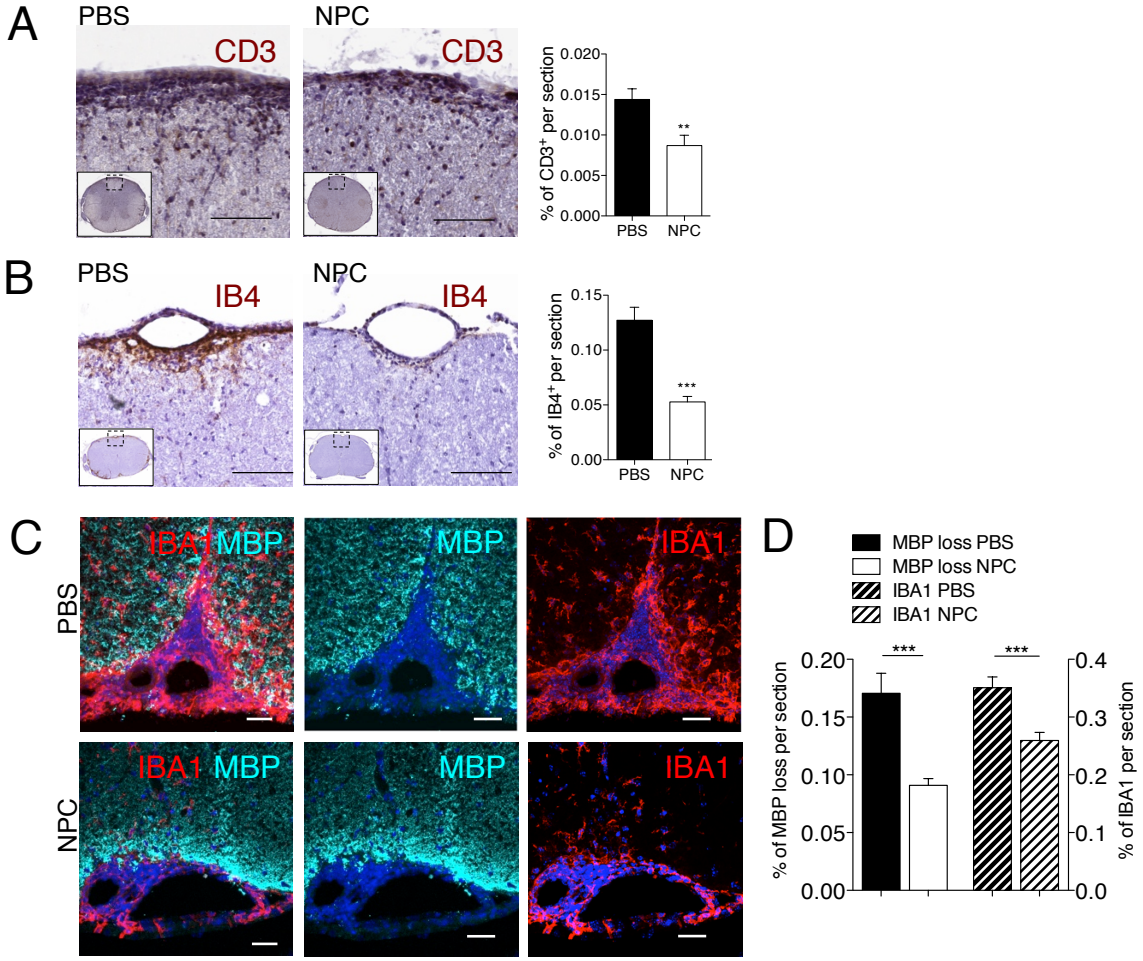

Supplemental Figure 1. Intrathecal NPC transplantation prevents the accumulation of inflammatory demyelinating lesions. (A-B) Representative images and quantification of T cells (immunohistochemistry for CD3) (A) and inflammatory phagocytes (immunohistochemistry for IB4) (B) at 30 dpi in respectively PBS- (black bars) vs NPC-treated (white bars), EAE mice (n=12-20 sections per mouse, 3 mice per group). (C-D) Representative immunofluorescence images (C) and quantification (D) of demyelination (area of MBP^+ loss) and inflammation (area of $IBA1^+$) in spinal cord sections of PBS- and NPC-treated EAE mice at 2 weeks post-transplantation (n=8-12 sections per mouse; n=3-4 mice per group). Data are mean±SEM and represent the percentage area of damage over total section area. *p≤0.05; **p≤0.01. Scale bars: A, 40 μm; C-D, 100 μm.

Supplemental Figure 2

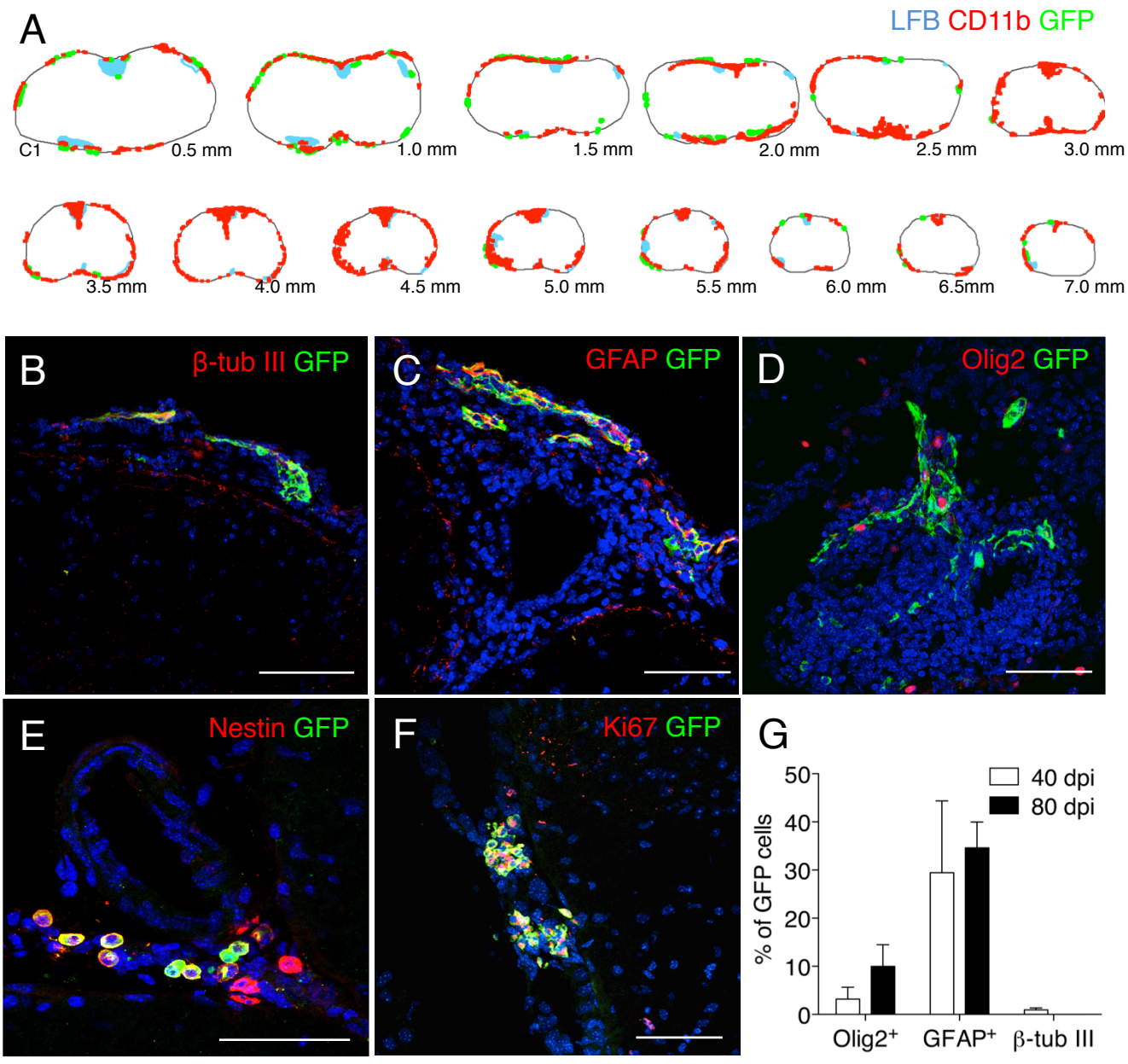

Supplemental Figure 2. Distribution and fate of intrathecally injected NPCs in EAE. (A) Representative serial 2D reconstruction of the distribution of demyelinating lesions (Luxol fast blue- LFB- staining, shown as blue line), transplanted GFP^+ NPCs (green dots) and $CD11b^+$ myeloid cells (red dots) in the cervical spinal cord (outlined with a grey line) in an NPC-treated mouse at 7 days post-transplantation (30 dpi) obtained from n=14 sequential stereology sections 500 μm apart starting from C1 (coordinates are indicated below each section). (B-F) Representative immunofluorescence images of GFP^+ NPCs (in green), 2 weeks after intrathecal transplantation (40 dpi) in EAE mice, co-expressing β-tubulin III (red in B), GFAP (red in C), Olig2 (red in D), Nestin (red in E) or Ki67 (red in F). Nuclei stained in DAPI are in blue. Scale bars in B- F, 25 μm. (G) Percentage of NPCs expressing the neural differentiation markers at the same time point (40 dpi) and at the end of the follow-up (80 dpi) (n=3 mice per group). Data are mean ±SEM.

Supplemental Figure 3

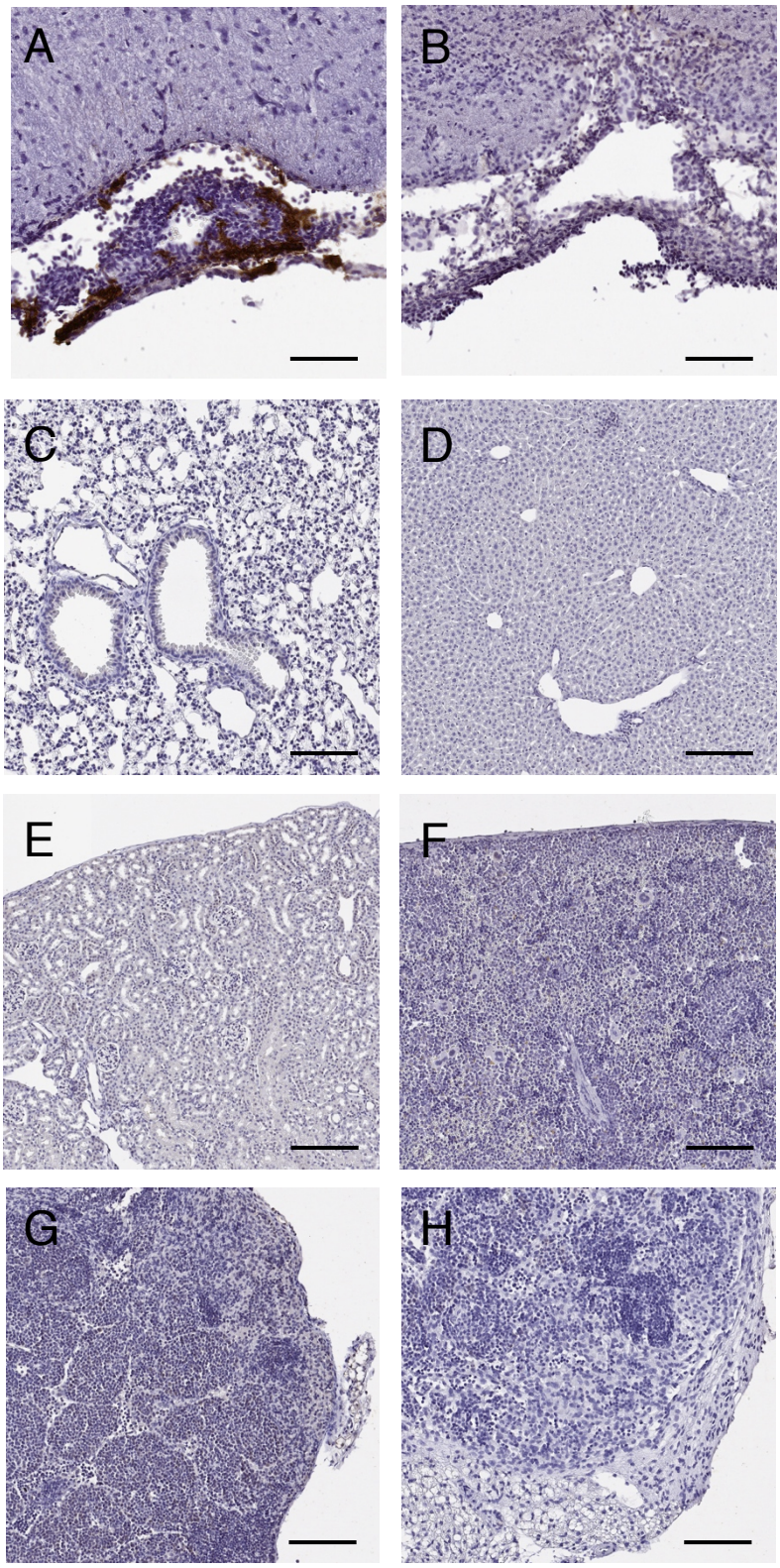

Supplemental Figure 3. Intrathecally injected NPCs are mostly localized in the subarachnoid space of the CNS and are not retrieved in secondary lymphoid organs and peripheral organs. (A) Representative diaminobenzidine (DAB) immunohistochemistry showing the prevalent localization of GFP^+ NPCs (in brown) in the subarachnoid space of the CNS of EAE mice (n=4) sacrificed 7 days after an intrathecal injection of 10^6 GFP^+ NPCs. (B) CNS of PBS-treated EAE mice was used as negative control to rule out non-specific DAB signal in the CNS meninges. (C-H) GFP^+ NPCs were not detected either in the parenchyma of filter organs (C, lung; D, spleen; E, kidney) or secondary lymphoid organs (F, spleen; G, deep cervical lymph-nodes; H, axillar lymph-nodes) of EAE mice (n=4) sacrificed 7 days after an intrathecal injection of 10^6 GFP^+ NPCs. Nuclei are counterstained with haematoxylin. Scale bars: A and B, 80μm; C-E, 200μm; F and G, 150μm; H, 100μm.

Supplemental Figure 4

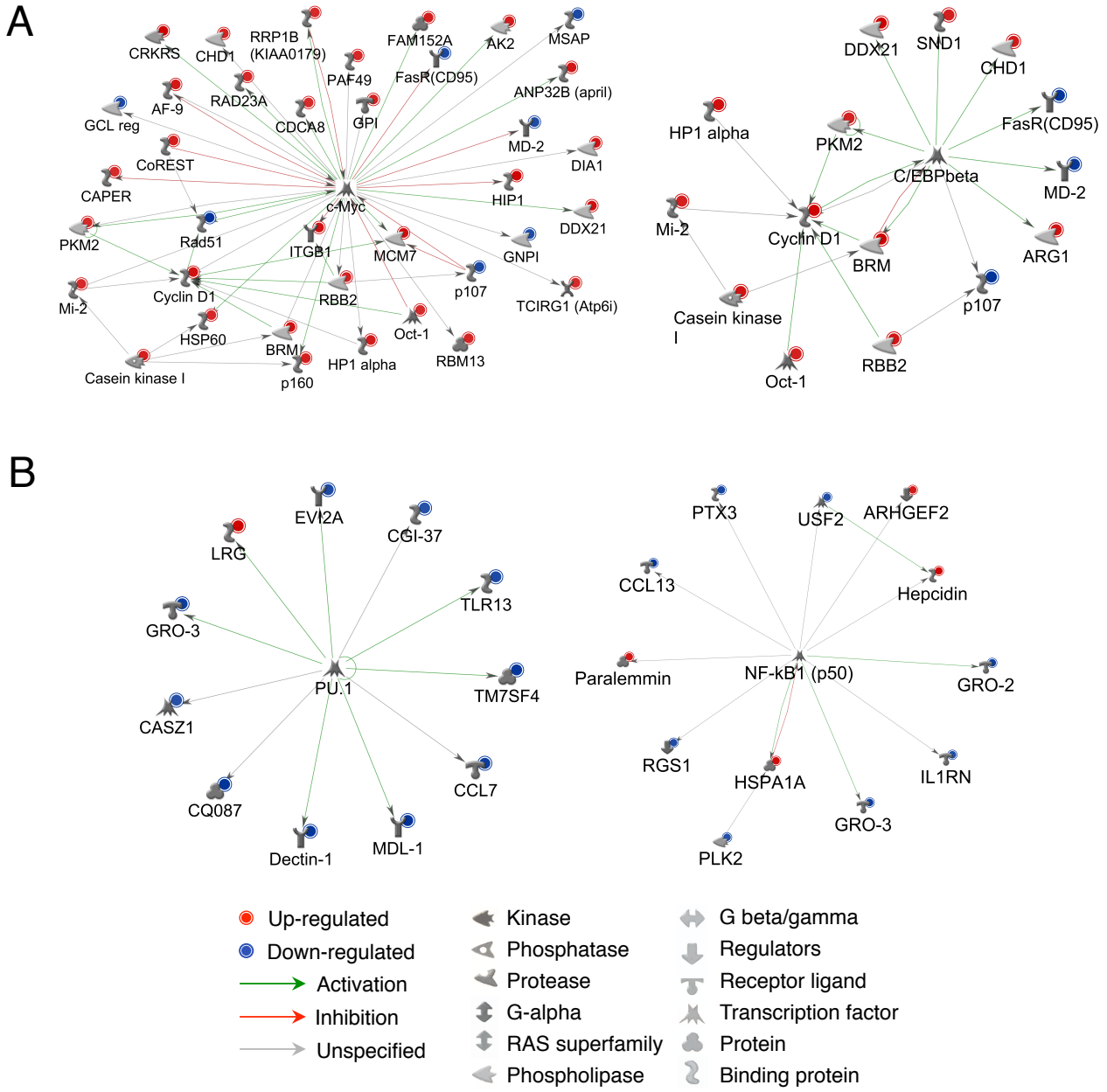

Supplemental Figure 4. Transcription factor networks in CD40L-maturing DCs conditioned with NPC-secreted factors. (A, B) Network analyses of the top enriched transcription factors at transcription factor analysis performed by *Metacore* (FDR ≤0.05) on differentially expressed genes between CD40L stimulated BMDCs (mDC) and CD40L stimulated BMDCs in presence of NCM (mDC-NCM) at indicated time points in culture. (A) Illustration of c-Myc (on the left) and c/EBPβ (on the right) networks in mDC-NCM (at 6h). (B) Illustration of PU.1 (on the left) and NF-kB1 (on the right) networks in mDC-NCM (at 18h) (see Figure 8A-B and Supplemental Table 1 and 2).

Supplemental Figure 5

A

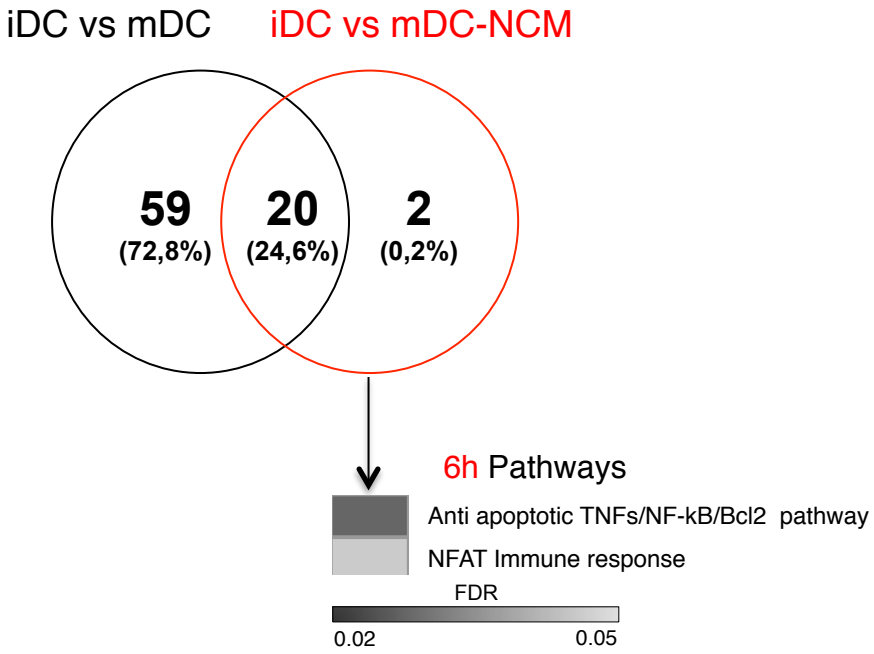

B

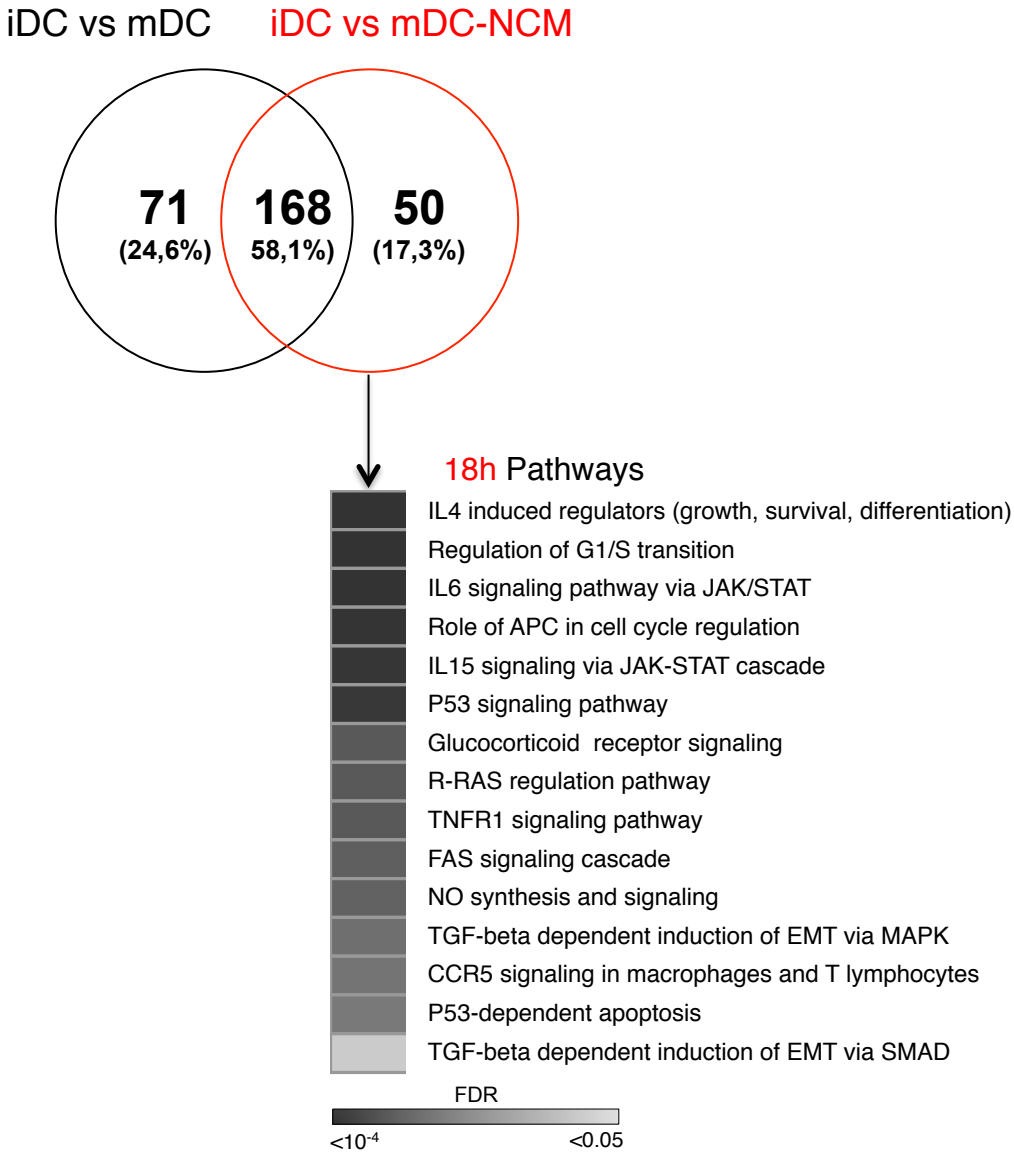

Supplemental Figure 5. Unique pathways modulated in NCM-conditioned BMDC maturation. (A, B) Overlapping pathways (*Metacore*; FDR≤0.05) enriched in the gene set obtained by comparing differential gene expression of immature BMDCs (iDC) versus CD40L-stimulated BMDCs (mDC) and immature BMDCs (iDC) versus BMDCs stimulated with CD40L in presence of NCM (mDC-NCM). List of pathways exclusively modulated in mDC-NCM at 6h or 18h are shown as grey scale reporting FDR in (A) and (B), respectively.

Supplemental Figure 6

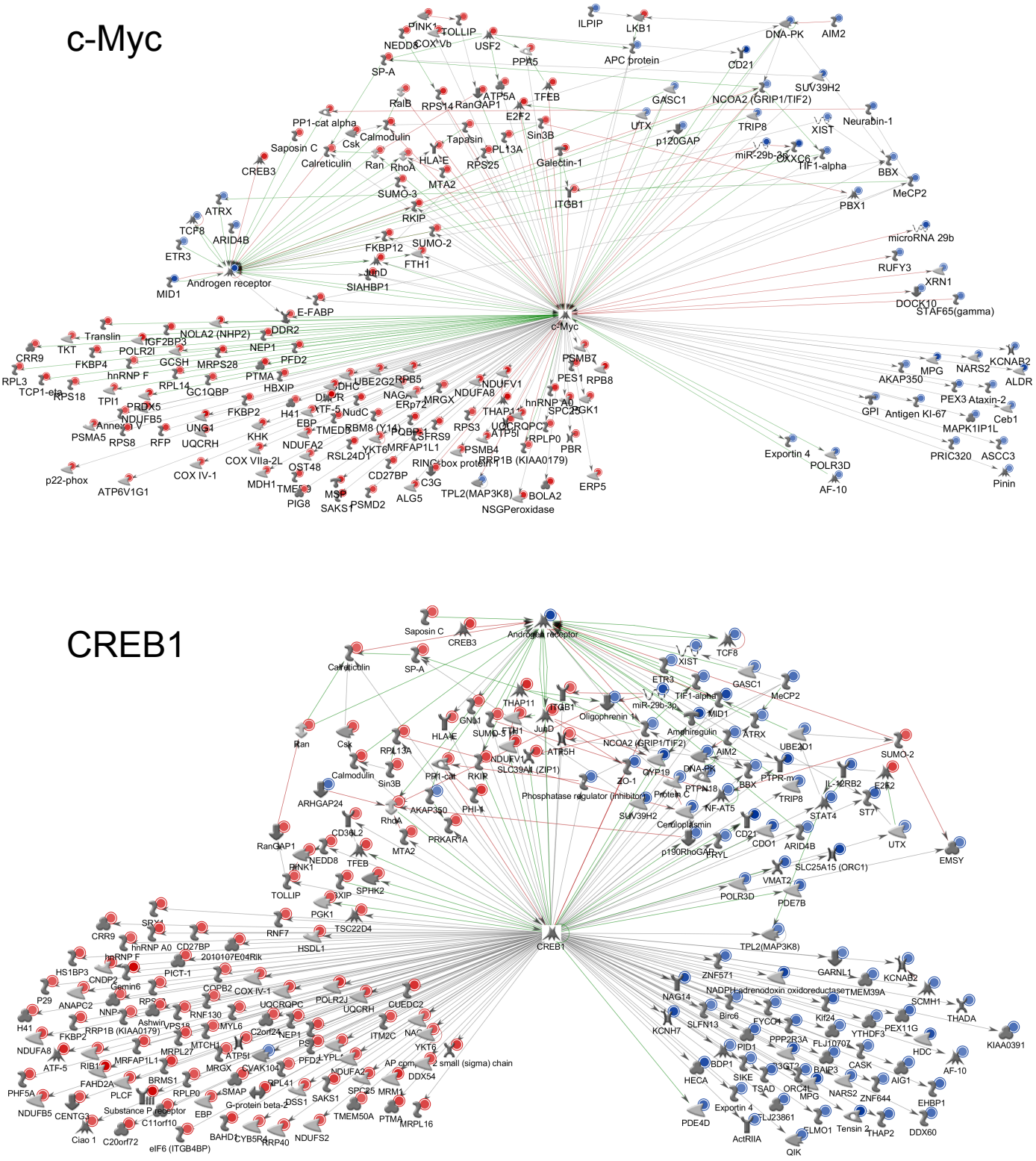

Supplemental Figure 6. Transcription factor networks of MCs in NPC-treated EAE mice. Illustration of c-Myc and CREB1 networks identified as the main regulators of the 610 NPC-modulated genes (see Figure 7A-B and Supplemental Table 3 and 4) with FDR≤0.05 at *Metacore* transcription factor analysis.

Supplemental Figure 7

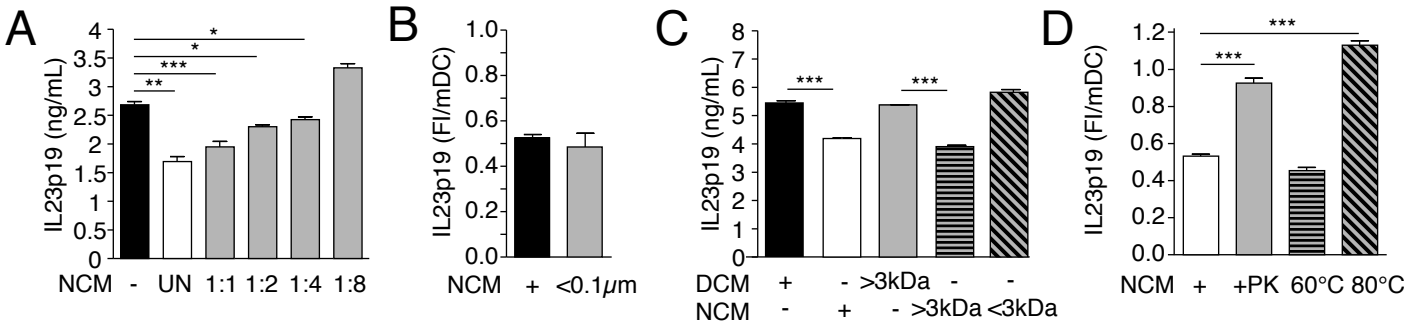

Supplemental Figure 7. Biochemical analysis of NPC-secreted factors. (A-D) Quantification by ELISA of IL23p19 secreted in the supernatant of CD40L-stimulated BMDCs cultured for 48h in absence or presence of NCM. Biochemical characterization of NCM was carried out with the following assays. (A) Dilution assay: mDC cultured either in control medium (black bar), undiluted NCM (white bar) or in doubling dilution of NCM (grey bars). (B) Size assay: mDC cultured either in whole or NCM filtered through a 0.1 μm mesh. (C) Molecular weight assay: mDC cultured in control medium (black bar), in unfractioned NCM (white bar), in the control medium fraction with a molecular weight greater than 3kDa (horizontal striped grey bar), in the NCM fraction with a molecular weight greater than 3kDa (grey striped bar) or in the NCM fraction with a molecular weight lower than 3kDa (grey oblique striped bar). (D) Temperature/enzymatic assay: IL23p19 production by mDCs cultured either in untreated (white bar) or proteinase K-treated NCM (grey bar) or heat-treated NCM for 30 min at 60°C (grey striped bar) or at 80°C (oblique striped grey bar). Data in A and B are reported as Fold Induction (FI) relative to mDC matured in DC control medium. *$p \leq 0.05$, **$p \leq 0.01$, ***$p \leq 0.001$, unpaired t-test. Data are mean ± SEM and are representative of two independent experiments.

Supplemental Figure 8

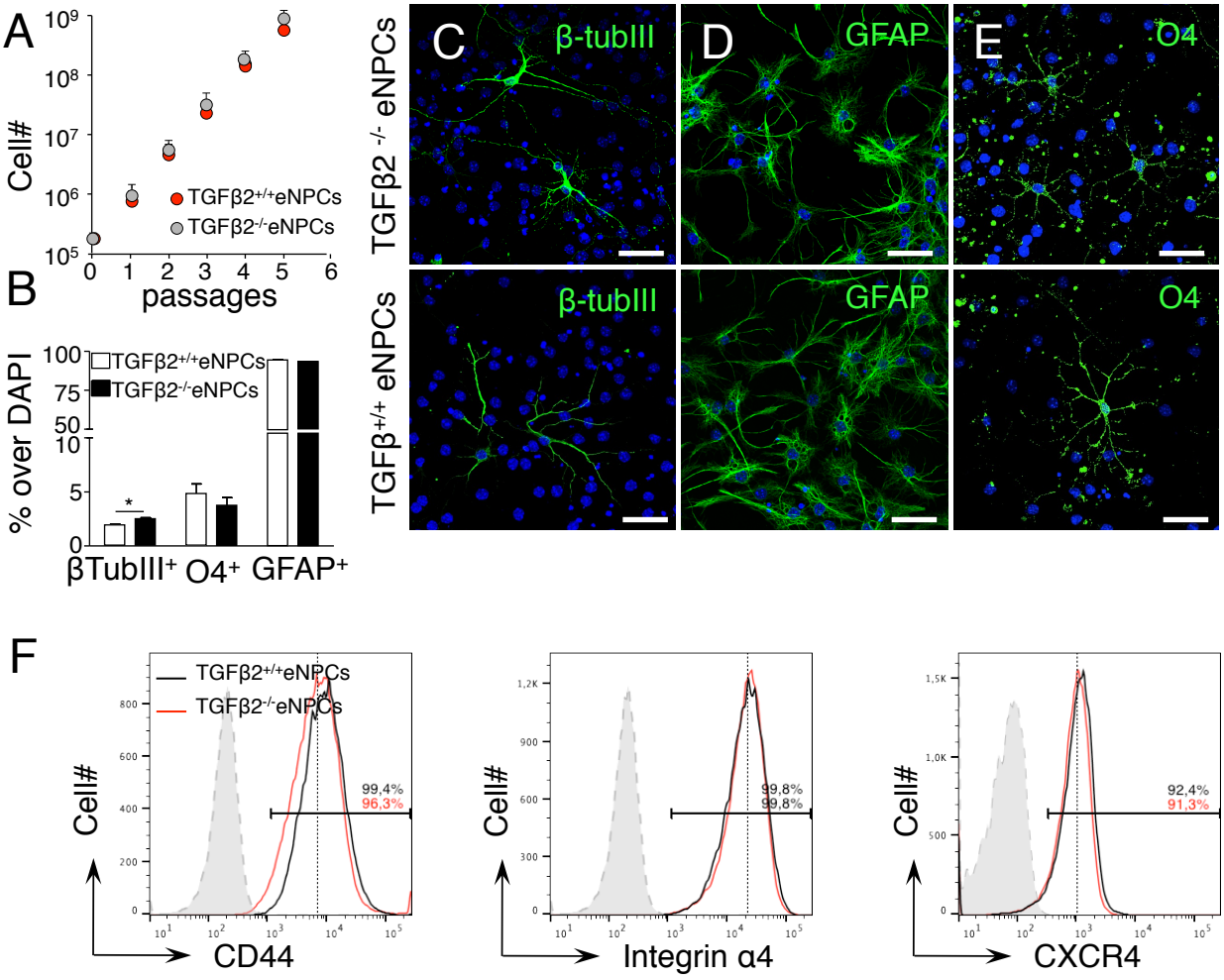

Supplemental Figure 8. *In vitro* characterization of *Tgfb2*$^{-/-}$ embryonic (E15.5) NPCs. (A) Growth curve of wt (*Tgfb2*$^{+/+}$ eNPCs) and *Tgfb2*$^{-/-}$eNPCs. (B-E) Quantification and representative immunofluorescence images of the differentiation of (*Tgfb2*$^{+/+}$) wt and *Tgfb2*$^{-/-}$ eNPCs in three neural-derived cell populations, neurons (C, β-tub III^{+} in green), astrocytes (D, GFAP^{+} in green) and oligodendrocytes (E, O4^{+} in green) upon growth factor withdrawal (see Methods). Nuclei stained with DAPI are in blue. Scale bar=50 μm. (F) Surface expression, evaluated by flow cytometry staining, of the adhesion molecule CD44, the chemokine receptor CXCR4 and the α4-integrin on *in vitro* cultured wt (black line) and *Tgfb2*$^{-/-}$ (red line) eNPCs are shown in histograms. Grey full histograms represent isotype controls. *p≤0.05, unpaired t-test. Data are mean ± SEM.

Supplemental Figure 9

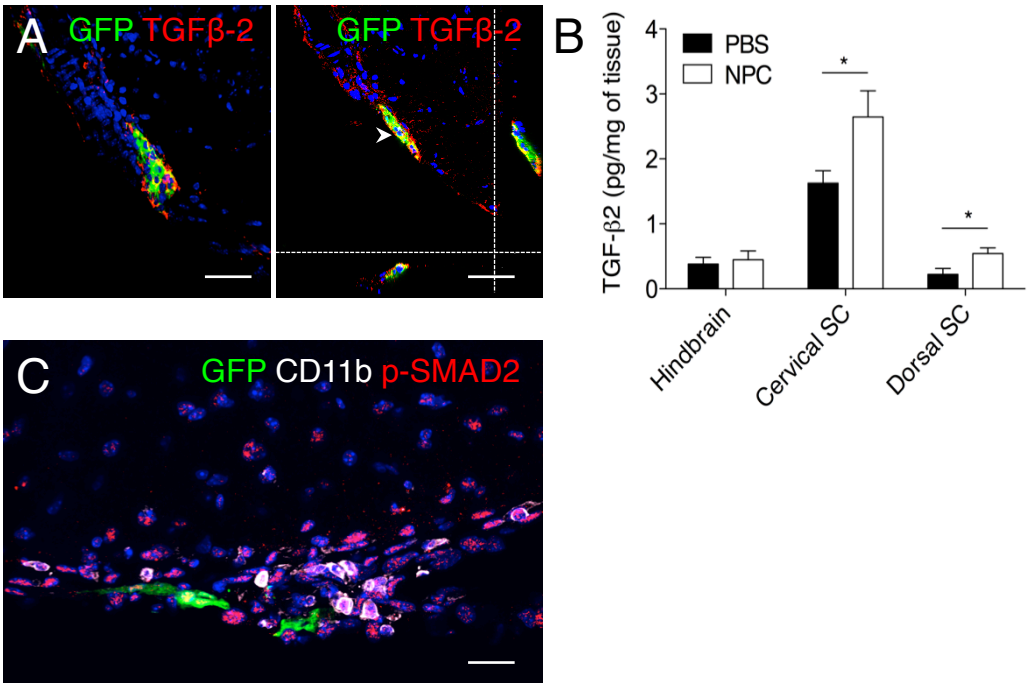

Supplemental Figure 9. Transplanted NPCs secrete TGF-β2 *in vivo* during the effector phase of EAE. (A) Representative confocal images for TGF-β2 (in red) and GFP^+ NPCs (in green) in spinal cord of EAE mice at 7 days after transplantation. The image on the left is shown on the right with the x-z (lower edge) and y-z (right edge) projection, separated by the dashed lines. Nuclei are stained with DAPI (in blue). Scale bar, 50 μm. (B) ELISA quantification of TGF-β2 in the CNS (hindbrain, cervical spinal cord and dorsal spinal cord) tissue of EAE mice either PBS-treated (PBS) or NPC-treated (NPC) (n=3-5 mice per group). *$p \leq 0.05$, unpaired t-test**.** (C) Representative confocal image for GFP^+ NPCs (in green), $CD11b^+$ (in white) myeloid cells and phospho-SMAD2 (p-SMAD2)$^+$ cells (in red) in spinal cord of EAE mice at 7 days after transplantation. Nuclei are stained with DAPI (in blue). Scale bar, 15 μm.

Supplemental Figure 10

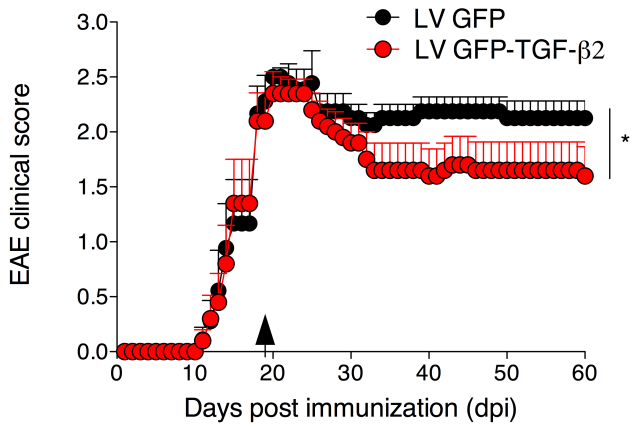

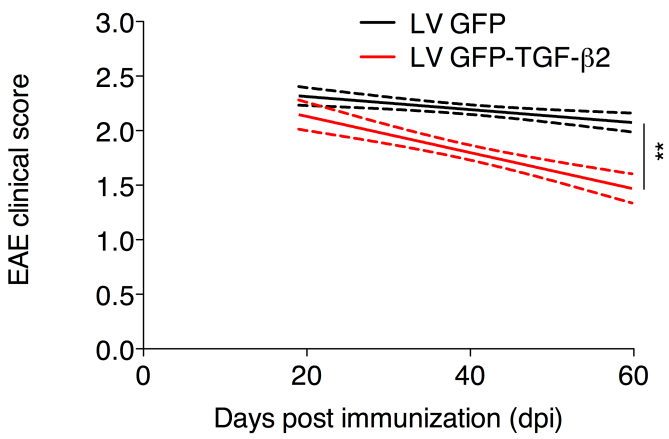

Supplemental Figure 10. Intrathecal TGF-β2 therapy ameliorates the chronic phase of EAE. Clinical scores of EAE mice treated with intrathecal injection of either control (GFP-expressing, black dots, n=8) or TGF-β2-expressing (red dots, n=10) lentiviral construct at the peak of the disease (4 day after the clinical onset) as indicated by the arrow. Each point represents the mean±SEM; *p≤0.05, two-way ANOVA with Bonferroni's post-test (left). Linear-regression curves (right) from day of treatment (19 dpi); dashed lines indicate 95% confidence interval. **p≤0.01.

SUPPLEMENTAL TABLES

Supplemental Table 1. List of differentially expressed genes with a fold change≥1.3 and p≤0.01 between CD40L-stimulated BMDCs in control medium (mDC) and in NCM (mDC-NCM) at 6h and 18h.

Supplemental Table 2. Transcription factor analysis (*Metacore*, FDR≤0.05) of differentially expressed genes between CD40L-stimulated BMDCs in control medium (mDC) and in NCM (mDC-NCM) at 6h and 18h.

Supplemental Table 3. List of the differentially expressed genes with p≤0.01 between MCs isolated from PBS- *vs* NPC-treated EAE mice at 7 days after intrathecal transplantation.

Supplemental Table 4. Transcription factor analysis (*Metacore*, FDR≤0.05) of differentially expressed genes between MCs isolated from PBS- *vs* NPC-treated EAE mice at 7 days after intrathecal transplantation.

SUPPLEMENTAL METHODS

Adult and embryonic mouse NPC culture and NCM preparation. Cells were cultured as neurospheres in NeuroCult® Proliferation kit (STEMCELL Technologies) containing 20 ng/ml of epidermal growth factor (EGF) and 10 ng/ml fibroblast growth factor (FGF) -II (Provitro). NPCs at passage number ≤ 10 were used in all experiments. All cells employed were tested and were negative for mycoplasma test (PCR).

For selected *in vivo* experiments, single cell-dissociated adult or embryonic NPCs were infected with 3 x 10^6 T.U./ml of two different third generation pCCLsin.PPT-hPGK lentiviral vectors (LV) engineered either with the GFP with nucleus/cytoplasm localization (#277) or with a farnesylated GFP (fGFP) with localization into the plasma membranes (#1514). The choice of an additional LV carrying the fGFP was made upon the need of specific membrane labelling for some *in vivo* experiments (e.g. looking at transplanted NPCs differentiating into myelin forming cells). Two days after LV infection, NPCs were harvested, centrifuged at 200g for 12 minutes and plated without further dissociation at a 1:1 ratio. After 2 passages of amplification *in vitro*, FACS analysis was performed to verify the efficiency of the infection (80-90%), as described (1, 2).

For multipotency assay (default differentiation into the three neural lineage), eNPCs were cultured on Matrigel-coated 16 mm-glass coverslips for 7 days in NeuroCult® Differentiation kit (STEMCELL Technologies) without growth factor, according to manufacturer's protocol.

Neural-stem cell conditioned medium (NCM) was obtained culturing 10^6 NPCs/ml in BMDC medium (see below) for 48 hours. The supernatant was centrifuged at 300*g* for 10 min, 0.2 μm-filtered to eliminate cell debris and stored at -20°C up to 2 months before being used in the indicated experiments. In specific experiments, NCM was filtered through a 0,1 μm filter (Millipore) just before application to BMDC cultures. For biochemical characterization of NCM, NCM and DC control medium were centrifuged through a 3kDa filter (Amicon-Ultra 4ml) for 45 minutes at 4000g. NCM eluate (≤3kDa) was supplemented with DCM retentate (≥3kDa) while NCM retentate (≥3Kda) was supplemented with DCM eluate (≤3kDa). The medium was then applied

to BMDC culture for 48 hours as previously indicated. As control we used DCM that underwent the same fractionation and reconstitution procedure as NCM.

Enzyme digestion of NCM was performed incubating NCM with 50 μg/ml proteinase K, for 1h at 37°C, followed by inactivation at 60°C for 30 min. For heat-inactivation assays, NCM was pre-heated at 60°C and 80°C for 30 min.

Microarray analysis. The raw data from mouse Illumina microarray on BMDCs unstimulated (iDC) or stimulated with CD40L in DCM (mDC) or NCM (mDC-NCM) at 6h and 18h of culture were background subtracted and cubic spine normalized using Illumina GenomeStudio software. Probe detection P-value analysis reported by the GenomeStudio was used as filtering criteria applying a threshold of $p \leq 0.01$. Two outlier samples (one from iDC 18h group and one from mDC-NPC 18h group) were found based on principal component analysis (PCA, R package) and excluded in the subsequent analyses. Differential gene expression analysis were performed in the R-bioconductor platform and the empirical Bayes test was used as implemented in the LIMMA package (3). Differentially Expressed Genes (DEG) with expression intensity≥100, P_{BH}-value ≤0.01 and ±1.3 fold change criteria were used for bioinformatic functional annotation using Metacore Gene Ontology, pathway and transcription factor enrichment analyses (http://thomsonreuters.com/metacore/). Heatmap was generated with GENE-E software.

NGS analysis. NGS of MCs ($CD45^{hi}CD11b^{+}Ly6C^{hi}Ly6G^{-}MHCII^{+}$) FACS sorted (7 days post-treatment) from the CNS of C57Bl/6 mice immunized and NPC- or PBS transplanted at the peak of EAE was performed on an Illumina NextSeq 500 System with TruSeq reagent kits and software. After removing adapters and low quality bases, sequence reads were aligned to the mouse reference genome (UCSC mm10) using STAR software (4). HTSeq-count (5) was then used to generate a list of the total number of uniquely mapped reads for each gene and sample. Sequence reads were normalized to library size using the Trimmed Median Means (TMM) in edgeR package (6). To determine which genes were differentially expressed between samples, the R package Limma was used (7). Genes with less than 1 cpm (count per milion reads) in at least 4 samples (1 replicate group) were removed from the data set. Voom was used to transform the count data to $\log_2$ counts per million and estimation

of the variance. The p value was set to a cut-off of 0.01, resulting in 610 significant, differentially expressed genes. Heatmap was generated with GENE-E software. Volcano plot was generated using limma. Gene set enrichment analyses were performed using Hallmark dataset in the MSigDatabase platform (Broad Institute). For Functional Enrichment Analysis Bipartite Graph: mouse modulated genes (p value ≤ 0.01) were transformed into their human orthologs using Biomart (8) and overlaps with GSEA hallmark pathways were computed using 'Compute Overlaps' online tool from the Broad Institute (http://software.broadinstitute.org/gsea/msigdb/annotate.jsp). Bipartite Graph was produced after importing enrichment results into Cytoscape. Transcription factor analysis has been done with Metacore (Thomson Reuters).

Histopathological analysis. Paraffin-embedded tissue sections (5 μm) were stained for Luxol fast blue to quantify demyelination and Bielschowsky silver impregnation and neurofilament staining to quantify axonal loss (n=15 sections per mouse; n=3-6 mice per group) as previously described (9-17). Frozen tissue sections (20 μm) were stained for hematoxilin-eosin, CD3 and IB4 to quantify total inflammatory infiltrate, T-cell infiltrate and macrophage infiltrate, respectively. For Luxol-fast blue, Bielschowsky and hematoxilin-eosin staining, tissue damage/immune cell infiltration was traced with ImageJ and expressed as the percentage of damage area/immune cell infiltration on the entire spinal cord section by a researcher blinded to the treatment scheme. Immunohistochemical stainings for neurofilament, IB4 and CD3 were performed utilizing the following reagents: mouse α-neurofilament 200 antibody (phosphorylated and non-phosphorylated, clone N52, Sigma, 1:400-1:800); isolectin B4 (BSI-B4, peroxidase conjugate, Sigma, 1:200); rabbit monoclonal αCD3 antibody (clone SP7, Abcam, 1:100). Images were then acquired using the Aperio Scanscope CS2 system (Leica Biosystems) and quantifications of the stained areas were performed by automated image analysis software with dedicated macros of the ImageScope program, customized according to manufacturer's instructions (Leica Biosystems). The representative images shown were identified within the total area of the analyzed sections and exported as ImageScope snapshots. For stainings at 30 dpi least 3 animals per group were analysed and 12 to 20 different rostro-caudal sections were analysed per animal. To assess the distribution of NPCs and $CD11b^+$ cells,

frozen tissue sections from brain and cervical SC from treated EAE animals, 7 days post transplantation, were serially sampled every 500 μm from -3.5 mm from bregma (starting from the first section positive for GFP^+NPCs) to the lower cervical spinal cord. NPCs were visualised by GFP immunohistochemistry. Demyelinating lesions were detected on consecutive sections by Luxol-fast-blue staining. Total cell number was assessed stereologically with Neurolucida and Stereo Investigator v 3.0 software (MicroBrightField, Inc., Colchester, VT, USA) and representative 3D and 2D reconstructions were obtained.

Immunofluorescence staining. Tissues were fixed with 4% paraformaldehyde in phosphate buffer solution (PBS) pH 7.2 and cryoprotected for at least 24h in 30% Sucrose (Sigma) in PBS at 4°C, prior to freezing in liquid nitrogen. Coronal brain and transverse spinal cord sections were then sampled by cryostat sections of 20 μm.

For cell immunofluorescence, cells were plated onto Matrigel-coated glass coverslips (16 mm^2) to adhere, prior to fixation in 4%PFA.

Both tissues and cells were incubated with blocking solution (goat serum 10% in PBS) for 1 h and then primary antibodies were applied in the same solution over night at 4 °C. For intracellular antigens, permeabilization with 0.05%-0.1% Triton-X was used.

The following primary antibodies were used: chicken αGFP (1:300, AB16901 Millipore); rabbit αvon Willebrand Factor (1:1000, Ab6994 Abcam); rat αCD45 (1:100, 550539 BD Pharmingen); rat αCD11b (1:100, MCA74GA AbD Serotec); rat αCD4 (1:200, 553043, BD Pharmigen), hamster αCD11c (1:500, 553800 BD Pharmingen), rabbit αGFAP (1:1500, Z0334 Dako); rabbit αKi67 (1:1000, NCL-KI67P Novocastra); rabbit αTuJ1 (1:1000, MMS-435P Covance); mouse αOlig2 (1:200, MABN50 Millipore), mouse αTGF-β2 (1:50 Ab36495 Abcam), rabbit α phospho-Smad2 (Ser465/467) (1:250, Ab3849 Millipore); rat αMBP (1:300, MAB386 Millipore); rabbit αIBA1 (1:400, 019-19741 WAKO). Appropriate fluorophore-conjugated secondary antibodies (Alexa Fluor 488, 546, 405 and 633, Molecular Probes) were used for detection. Nuclei were stained with 40,6-diamidino-2-pheny-lindole (DAPI, Roche). For CD11c, signal amplification was achieved with a

TSA Plus Cyanine 5 Kit (Perkin-Elmer). Images were acquired on the Leica confocal microscope TCS SP5 with a 40x and 63x oil- immersion objective.

For quantification of NPC differentiation *in vivo*, the total number of NPCs, as well as double-positive NPCs, were counted on sequential, 500-µm apart spinal cord and brain sections of n=3 treated mice both at 40 and 80 dpi. Double-positive cells were expressed as percentage over the total number of NPCs.

For quantification of the % of p-SMAD2 cells over $CD11b^+$ cells, p-$Smad2^+CD11b^+$ cells and $CD11b^+$ cells were counted in 8-12 images at the cervical spinal cord level (n= 3 mice per group) acquired on the Leica confocal microscope TCS SP5 with a 63x oil- immersion objective.

For quantification of the demyelination and inflammation 2 weeks post-treatment, spinal cord cryosections were stained by immunofluorescences for MBP and IBA1 and then acquired using the Vectra.3 200 slide scanner (Perkin Elmer). The quantification of the stained area was performed on 8-12 images of n=3-4 mice per group by automated image analysis software INFORM using a dedicated 'Tissue segmentation' algorithm, customized according to manufacturer's instructions (Perkin Elmer). The representative images were acquired on the Leica confocal microscope TCS SP5 with a 63x oil- immersion objective.

qPCR analysis. Total RNA was extracted from cells with RNeasy Mini Kit or Micro Kit (Qiagen). Genomic DNA was removed by treatment with DNase I (Qiagen). Complementary DNA (cDNA) was synthesized using the Superscript III reverse transcription kit (Invitrogen). qPCR was performed on a 7500 Fast Real Time PCR System (Applied Biosystems) using TaqMan Universal PCR Master Mix (Applied Biosystems). Primer assays were purchased from Applied Biosystems with the following primers and probes (from Applied Biosystems; identifier in parentheses): *Cxcl3* (Mm01701838_m1), *Csf2* (Mm01290062_m1), *Tbx21* (Mm00450960_m1), *Il22* (Mm00444241_m1), *Il23r* (Mm00519943_m1), *Rorc* (Mm00441144_g1), *Tgfb1* (Mm01178820_m1), *Tgfb2* (Mm00436955_m1), *Tgfb3* (Mm01307950_m1), *inhiba* (Mm00434339_m1), *acvr1* (Mm01331069_m1); acvr2 (Mm00431657_m1); *BMP2* (Mm01340178); *BMP4* (Mm00432087); *BMP7* (Mm00432087); *BMPr1a* (Mm00477650); *BMPr1b* (Mm00432117); *BMPr2 (*Mm00432134); *TGFβr1*

(Mm00436964); *TGFβr2* (Mm00436977); *CD80* (Mm00711660_m1); *CD86* (Mm00444543_m1); *il23a* (Mm01160011_g1); *CD36* (Mm01135198_m1); FoxP3, (Mm00475162_m1); *Arg1* (*Mm00475988_m1*); *Tnfa* (Mm00443258_m1); *Il1b* (Mm00440502_m1); *Il6* (Mm00446190_m1); *Arg1* (Mm00475988_m1); *Tgm2* (Mm00436987_m1); *Hspa1a* (Mm01159846_s1); *Ifitm6* (Mm01612924_g1); *Il33* (Mm00505399_m1); *Clec9a* (Mm00554956_m1); *Clec7a* (Mm00490960_m1); *Hamp* (Mm00519025_m1); *Pde2a*(Mm01136629_m1); *Stab1* (Mm00460390_m1); *Itch* (Mm00492683_m1); *Maf* (Mm02581355_s1); *Rad51* (Mm00487905_m1*); Fgf2* (Mm01285715_m1); *Itga5* (Mm00434486_m1); *Itgb8* (Mm00623991_m1); *Thbs1* (Mm00449032_g1); *Thbs2* (Mm01279240_m1); *Mmp2* (Mm00439498_m1); *Mmp9* (Mm00442991_m1); and *Gapdh* (4352339E). The comparative threshold cycle method and an internal control (*Gapdh*) were use for normalization of the target genes.

Vector construction and production. The plasmid pUNO1-mTGFB2 was purchased from Invivogen. The coding sequence of mouse TGF-β2 was cloned under the PGK promoter in a third generation bidirectional LV, expressing also the reporter gene GFP under CMV promoter, using standard cloning techniques.

Third-generation LVs were produced by calcium phosphate transient transfection of 293T cells of the selected transfer vector, the packaging plasmid pMDLg/p.RRE, pCMV.REV, the VSV-G envelope plasmid pMD2.G and the pAdVAntage plasmid (Promega), as previously described (18).

Vector titration. Serial dilutions of the virus were used to infect HEK293T cells in the presence of Polybrene (8 μg/ml, suspended in 10 ml of IMDM, Sigma). HEK293T cells were the plated at the density of $5x10^4$ cells/well a 6-wells plate for 24 hours. The medium was then removed and in each well were added a 500 μl of IMDM/Polybrene 2X plus 500 μl of IMDM with viral particles (serial dilutions ranging from 1: 10^3 to 1: 10^7). After 18 hours, 1 ml of fresh IMDM/well was added. The HEK293T cells were harvested after 5 days in vitro and analysed at the FACS, to determine the percentage of reporter (GFP)-expressing cells. The viral titre was expressed as Transducing Units (T.U.)/ml, which represents the number of vector genomes infecting, entering and integrating into a given population of cells and calculated using the formula: Viral Titre = [(% GFP+ cells x 100,000 plated cells)/100] x virus dilution factor.

LV injection. At the treatment day 4 days after clinical onset of EAE, animals were randomized into treatment groups and injection of TGFβ2-expressing or GFP expressing LV (2 x 10^7 TU/mL) was performed with the same protocol described for **NPC intrathecal transplantation**.

SUPPLEMENTAL REFERENCES

1. Pluchino S, Zanotti L, Brambilla E, Rovere-Querini P, Capobianco A, Alfaro-Cervello C, Salani G, Cossetti C, Borsellino G, Battistini L, et al. Immune regulatory neural stem/precursor cells protect from central nervous system autoimmunity by restraining dendritic cell function. *PLoS One*. 2009;4(6):e5959.
2. Pluchino S, Zanotti L, Rossi B, Brambilla E, Ottoboni L, Salani G, Martinello M, Cattalini A, Bergami A, Furlan R, et al. Neurosphere-derived multipotent precursors promote neuroprotection by an immunomodulatory mechanism. *Nature*. 2005;436(7048):266-71.
3. Smyth GK. Linear models and empirical bayes methods for assessing differential expression in microarray experiments. *Stat Appl Genet Mol Biol*. 2004;3(Article3.
4. Dobin A, Davis CA, Schlesinger F, Drenkow J, Zaleski C, Jha S, Batut P, Chaisson M, and Gingeras TR. STAR: ultrafast universal RNA-seq aligner. *Bioinformatics*. 2013;29(1):15-21.
5. Anders S, Pyl PT, and Huber W. HTSeq--a Python framework to work with high-throughput sequencing data. *Bioinformatics*. 2015;31(2):166-9.
6. Robinson MD, McCarthy DJ, and Smyth GK. edgeR: a Bioconductor package for differential expression analysis of digital gene expression data. *Bioinformatics*. 2010;26(1):139-40.
7. Ritchie ME, Phipson B, Wu D, Hu Y, Law CW, Shi W, and Smyth GK. limma powers differential expression analyses for RNA-sequencing and microarray studies. *Nucleic Acids Res*. 2015;43(7):e47.
8. Smedley D, Haider S, Durinck S, Pandini L, Provero P, Allen J, Arnaiz O, Awedh MH, Baldock R, Barbiera G, et al. The BioMart community portal: an innovative alternative to large, centralized data repositories. *Nucleic Acids Res*. 2015;43(W1):W589-98.
9. Basso AS, Frenkel D, Quintana FJ, Costa-Pinto FA, Petrovic-Stojkovic S, Puckett L, Monsonego A, Bar-Shir A, Engel Y, Gozin M, et al. Reversal of axonal loss and disability in a mouse model of progressive multiple sclerosis. *J Clin Invest*. 2008;118(4):1532-43.
10. Gruber RC, Ray AK, Johndrow CT, Guzik H, Burek D, de Frutos PG, and Shafit-Zagardo B. Targeted GAS6 delivery to the CNS protects axons from damage during experimental autoimmune encephalomyelitis. *J Neurosci*. 2014;34(49):16320-35.
11. Jakubzick CV, Randolph GJ, and Henson PM. Monocyte differentiation and antigen-presenting functions. *Nat Rev Immunol*. 2017;17(6):349-62.
12. Konkel JE, Zhang D, Zanvit P, Chia C, Zangarle-Murray T, Jin W, Wang S, and Chen W. Transforming Growth Factor-beta Signaling in Regulatory T Cells Controls T Helper-17 Cells and Tissue-Specific Immune Responses. *Immunity*. 2017;46(4):660-74.
13. Kuboyama K, Fujikawa A, Masumura M, Suzuki R, Matsumoto M, and Noda M. Protein tyrosine phosphatase receptor type z negatively regulates oligodendrocyte differentiation and myelination. *PLoS One*. 2012;7(11):e48797.
14. Montarolo F, Raffaele C, Perga S, Martire S, Finardi A, Furlan R, Hintermann S, and Bertolotto A. Effects of isoxazolo-pyridinone 7e, a potent activator of

the Nurr1 signaling pathway, on experimental autoimmune encephalomyelitis in mice. *PLoS One*. 2014;9(9):e108791.
15. Pluchino S, Quattrini A, Brambilla E, Gritti A, Salani G, Dina G, Galli R, Del Carro U, Amadio S, Bergami A, et al. Injection of adult neurospheres induces recovery in a chronic model of multiple sclerosis. *Nature*. 2003;422(6933):688-94.
16. Pryor WM, Freeman KG, Larson RD, Edwards GL, and White LJ. Chronic exercise confers neuroprotection in experimental autoimmune encephalomyelitis. *J Neurosci Res*. 2015;93(5):697-706.
17. Spath S, Komuczki J, Hermann M, Pelczar P, Mair F, Schreiner B, and Becher B. Dysregulation of the Cytokine GM-CSF Induces Spontaneous Phagocyte Invasion and Immunopathology in the Central Nervous System. *Immunity*. 2017;46(2):245-60.
18. Follenzi A, and Naldini L. HIV-based vectors. Preparation and use. *Methods Mol Med*. 2002;69(259-74.